Thermal effects of internal gravity waves in the Martian upper atmosphere

Alexander S. Medvedev[1] and Erdal Yiğit[2,3,4]

Received 4 January 2012; revised 7 February 2012; accepted 9 February 2012; published 9 March 2012.

[1] For the first time, gravity wave-induced heating and cooling effects were fully and interactively incorporated into a Martian general circulation model (GCM). Simulations with a comprehensive GCM with an implemented spectral nonlinear gravity wave (GW) parameterization revealed significant thermal effects of GWs in the mesosphere and lower thermosphere (MLT) between 100 and 150 km. Wave-induced heating and cooling rates are comparable with those due to near-IR CO_2 heating and IR CO_2 cooling, correspondingly. Accounting for thermal effects of GWs results in a colder simulated MLT, with the most of cooling taking place in middle- and high-latitudes. In the winter hemisphere, the temperature decrease can exceed 45 K. The colder simulated MLT is in a good agreement with the SPICAM stellar occultation measurements and Mars Odyssey aerobraking temperature retrievals. Our experiments suggest that thermal effects of GWs are probably a key physical mechanism in the MLT missing in contemporary Martian GCMs. **Citation:** Medvedev, A. S., and E. Yiğit (2012), Thermal effects of internal gravity waves in the Martian upper atmosphere, *Geophys. Res. Lett.*, *39*, L05201, doi:10.1029/2012GL050852.

1. Introduction

[2] Gravity waves (GWs) are ubiquitous in the Martian atmosphere. They are excited in the lower atmosphere by flow over the rugged topography, instabilities of weather systems, volatile convection, and are modulated by tides. Measurements through radio occultation [*Creasey et al.*, 2006a] and accelerometry [*Magalhães et al.*, 1999; *Creasey et al.*, 2006a, 2006b; *Fritts et al.*, 2006] indicate that Martian GW amplitudes and the associated momentum fluxes are several times larger than those on Earth. *Fritts et al.* [2006] and *Heavens et al.* [2010] inferred an appreciable body forcing of several thousand m s^{-1} sol^{-1} produced by GWs upon their saturation and breaking in the upper atmosphere. Dynamical effects of these waves were studied using Martian general circulation models (GCMs) with earlier parameterizations of GWs including only orographically-generated harmonics with zero horizontal phase speed and simplified Lindzen-type breaking criterion [*Joshi et al.*, 1995; *Collins et al.*, 1997, and references therein]. They demonstrated some importance of GWs near the edge of the westerly jet in the winter hemisphere, where the induced drag varies from tens to hundreds of m s^{-1} sol^{-1}. "Orographic" GW schemes are now routinely used in some Martian GCMs. They either show a limited contribution of only ≈10% of the forcing due to resolved-scale eddies [*Hartogh et al.*, 2005], or do not appear to impact the middle atmosphere [*Angelats i Coll et al.*, 2005]. Our recent GCM modeling with an implemented spectral GW parameterization that encompasses harmonics with non-zero phase velocities revealed a significant dynamical influence of small- to medium-scale gravity waves (with characteristic horizontal wavelengths of 200–300 km) in the Martian mesosphere and lower thermosphere (MLT) [*Medvedev et al.*, 2011a, 2011b]. In particular, they strongly weaken the easterly (retrograde) winds, close up both easterly and westerly jets around 100–130 km, and alter the meridional circulation.

[3] Unlike with the dynamical impact, thermal effects of GWs on Mars were studied to a much lesser degree. These effects include a) heating of the mean flow due to an irreversible conversion of mechanical wave energy into heat [*Becker and Schmitz*, 2002; *Medvedev and Klaassen*, 2003], and b) differential heating/cooling due to a divergence of the induced downward sensible heat flux [*Walterscheid*, 1981; *Medvedev and Klaassen*, 2003; *Becker*, 2004]. The latter is the result of altering the phase relationship between fluctuations of temperature and vertical velocity in dissipating harmonics. In the terrestrial MLT, the thermal effects of GWs are appreciable [*Medvedev and Klaassen*, 2003], while in the thermosphere above the turbopause they are extremely significant: the irreversible heating is of the order of magnitude of the Joule heating, and the differential cooling can compete with that due to molecular heat conduction in the *F* region [*Yiğit and Medvedev*, 2009]. On Mars, *Parish et al.* [2009] studied the impact of GW drag and thermal effects on the thermosphere using a 1-D linear wave model. They have found that the associated heating and cooling can reach 70–300 K sol^{-1} at 135–175 km at the northern winter solstice.

[4] This paper is the first study that fully and interactively incorporates thermal effects of saturating/breaking GWs in a 3-D Martian GCM. Its timeliness is underscored by the current understanding that Martian GCMs "may be missing some important physical process(es) that is preventing … models from reproducing the [observed] mesopause temperature" [*McDunn et al.*, 2010]. Our study is based on the simulations with a Martian GCM interactively coupled with a parameterization of subgrid-scale GWs. This scheme considers wave propagation in a dissipative atmosphere, which the Martian upper atmosphere is, takes into account

[1]Max Planck Institute for Solar System Research, Katlenburg-Lindau, Germany.
[2]Department of Atmospheric, Oceanic and Space Sciences, University of Michigan, Ann Arbor, Michigan, USA.
[3]Atmospheric Physics Laboratory, Department of Physics and Astronomy, University College London, London, UK.
[4]Space Sciences Laboratory, University of California, Berkeley, California, USA.

0094-8276/12/2012GL050852

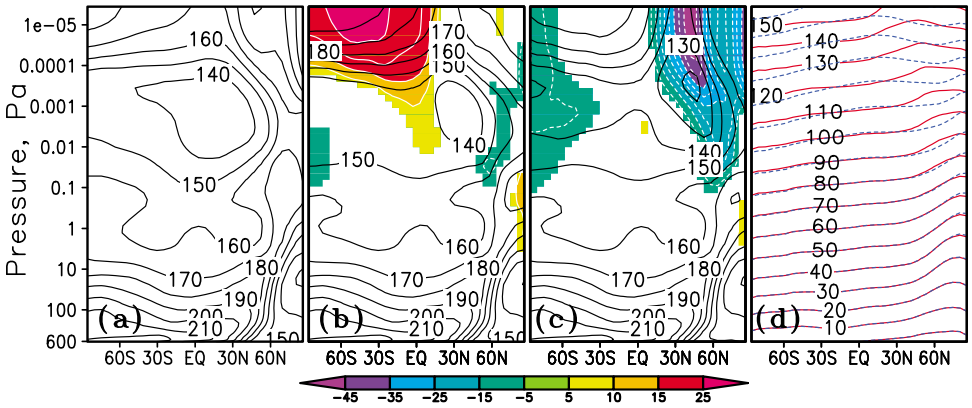

Figure 1. Zonal mean temperature (black contour lines) on L_s = 270° simulated (a) without accounting for unresolved GWs, (b) with the parameterized GW dynamical forcing only, and (c) with both dynamical and thermal effects included in the GW parameterization. Shaded are the temperature differences between the corresponding run and the simulation without GW parameterization shown in Figure 1a. Figure 1d shows zonally averaged geopotential heights for runs a and c in blue and red, correspondingly.

nonlinear interactions between harmonics leading to saturation and/or breaking, refraction, critical level filtering, and damping by molecular diffusion and heat conduction. The scheme was described in full detail by *Yiğit et al.* [2008], and extensively tested in the Earth's GCM [*Yiğit et al.*, 2009, 2012; *Yiğit and Medvedev*, 2009, 2010] as well as in the Martian context [*Medvedev et al.*, 2011a, 2011b]. The GCM, GW parameterization, and design of numerical experiments are outlined in section 2. Results are presented in section 3, and implications for the thermospheric winter polar warming [*Bougher et al.*, 2006] are discussed in section 4. The comparison of GW-induced heating/cooling rates with those due to main thermal forcing mechanisms in the Martian MLT is given in section 5.

2. Model, Gravity Wave Scheme, and Simulation Design

[5] The Martian GCM used in this study is described in detail in the work of *Medvedev et al.* [2011b] and the earlier papers [*Hartogh et al.*, 2005; *Medvedev and Hartogh*, 2007]. Since the main GW effects have been found in the upper atmosphere above 100 km [*Medvedev et al.*, 2011b], the model top in the present version of the GCM was raised somewhat higher to p = $3.6 \cdot 10^{-6}$ Pa (≈150–160 km). Additionally, a parameterization of heating due to absorption of solar UV and EUV by CO_2 molecules was introduced. The latter includes 37 spectral intervals ranging from 5 to 105 nm [*Torr et al.*, 1979], employs the solar EUV flux model of *Richards et al.* [1994], and the heating efficiency was assumed equal to 0.22 following the work of *González-Galindo et al.* [2005]. All simulations to be presented below were performed on 67 hybrid vertical levels with T21 horizontal spectral truncation (36 and 64 grid points in longitude and latitude, respectively) for perpetual Northern Hemisphere winter (L_s = 270°). The dust and solar activities were kept low and constant to eliminate possible uncertainties with their variations. The dust optical depth in visible was uniformly preset at τ = 0.2, and the solar activity corresponded to $F_{10.7} = 80 \times 10^{-22}$ W m^{-2} Hz^{-1} at the Earth orbit.

[6] The GW scheme and its setup were described by *Medvedev et al.* [2011b, and references therein]. 28 harmonics with horizontal phase speeds c_i from −60 to 60 m s^{-1} were launched at p = 260 Pa (≈8 km) along the direction of local wind at the source level, both up- ($c_i < 0$) and down the wind ($c_i > 0$). The amplitudes of horizontal momentum fluxes were distributed normally, and the normalizing coefficient was chosen such that the rms wave fluctuations of horizontal velocity were close to 1 m s^{-1}. From the equipartition of wave kinetic $E_k = \overline{u'^2}/2$ and potential energy per unit mass, E_p, this corresponds to the background value of $E_p \approx 0.5$ J kg^{-1} inferred by *Creasey et al.* [2006a, Figure 5] in the lower atmosphere of Mars. Vertical propagation of individual harmonics with horizontal phase speed c_i and the resulting momentum deposition rate a_i were calculated for all grid points. The thermal effect of a harmonic is the sum of heating due to an irreversible wave dissipation, Q^i_{irr}, and the differential heating/cooling, Q^i_{dif}, associated with the divergence of wave-induced heat flux [*Medvedev and Klaassen*, 2003, equation 36′]:

$$Q^i_{irr} = c_p^{-1} a_i (c_i - \bar{u}), \qquad Q^i_{dif} = \frac{H}{2\rho R}\frac{\partial}{\partial z}[\rho a_i (c_i - \bar{u})], \qquad (1)$$

where c_p is the specific heat at constant pressure, a_i is momentum deposition rate (acceleration or deceleration), $\bar{u}$ is the local wind, H is the density scale height, R is the gas constant, and ρ is the background mass density. Unlike in our previous work [*Medvedev et al.*, 2011b], the thermal forcing originating from all GW harmonics was included in the thermodynamic equation for resolved fields. Along with the multiple-wave parameterization outlined above, an "orographic" GW scheme for harmonics $c_i = 0$ is included as a part of the "standard" model, as described by *Hartogh et al.* [2005]. It relies upon the subgrid-scale variations of topography for specifying wave sources at the lower boundary. Thermal effects of such waves are computed in a similar way.

3. Temperature Changes

[7] Three numerical experiments are compared here: 1) the benchmark run without parameterized GWs, 2) with only

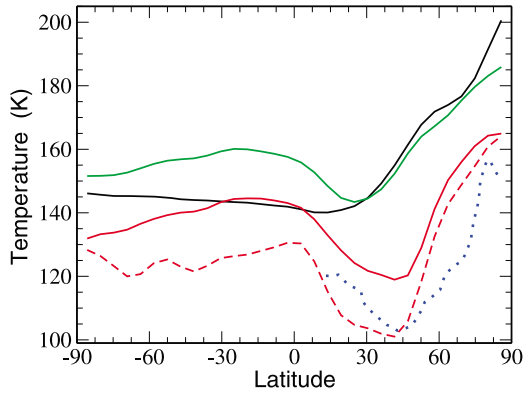

Figure 2. Zonally and diurnally averaged temperatures (solid lines) at p = 0.0002 Pa (≈120 km) from the runs without GWs (black), with only dynamical effects of GWs ("drag") included (green), and with both dynamical and thermal effects accounted for (red). The blue dotted line presents the night-time temperature inferred from ODY aerobraking measurements [*Bougher et al.*, 2006]. The red dashed line corresponds to the night-time (near 02:00 hours) temperature from the run including both dynamical and thermal GW effects.

dynamical effects of GWs ("drag"), and 3) with both dynamical and thermal effects included. The model was run in the perpetual mode for 90 sols to reach a quasi-equilibrium followed by an averaging over the last 5 sols. Zonal and meridional wind patterns simulated in the first two runs are very similar to those described in our previous paper [*Medvedev et al.*, 2011b] despite the addition of the EUV heating, and, therefore, are not shown here. Accounting for the thermal effects of GWs in the run 3 did not modify the simulated winds significantly compared to the run 2. More worthy of presentation are the temperature fields in Figure 1.

[8] Unlike in the work by *Medvedev et al.* [2011b], all three presented runs reproduce the mesopause between 0.001 and 0.0001 Pa (100 to 130 km) caused entirely by the inclusion of the EUV heating parameterization. The color shaded differences between the corresponding runs and the benchmark demonstrate a significant influence of GWs. Figure 1b shows up to 25 K warming in the Southern lower thermosphere, enhancement of the winter polar warming in the lower atmosphere, and up to 10 K cooling above. These changes are the result of altering the meridional circulation purely by GW drag. It should be emphasized that the very same GW forcing produced a more than 20 K higher temperature in the MLT over the Northern Pole when EUV heating was not included [*Medvedev et al.*, 2011b, Figure 9]. This may serve as an indication that the thermospheric winter polar warmings [*Bougher et al.*, 2006] are created by a mechanism unrelated to GWs, and depend on the latter only weakly.

[9] Accounting for thermal effects of GWs (Figure 1c) introduces spectacular changes. The temperature in middle- and high-latitudes in both hemispheres becomes colder, especially in the winter hemisphere, where it drops by more than 45 K compared to the simulation without parameterized GWs altogether. These overall colder (although not uniform with latitude) temperatures in the Martian MLT are consistent with the stellar occultation measurements of *Forget et al.* [2009], who found that the temperatures in the 100–130 km layer were systematically colder than expected from a GCM, [e.g., *González-Galindo et al.*, 2009; *McDunn et al.*, 2010].

[10] In the middle atmosphere below ≈70–90 km, the dynamical impact of GWs on the temperature field dominates the thermal effects. The lower shaded regions over the North Pole in Figures 1b and 1c indicate an enhancement of the polar warming by the parameterized GWs. The magnitude and location of thus simulated temperature maximum agree well with the measurements from Mars Climate Sounder onboard the Mars Reconnaissance Orbiter (MRO–MCS) for low-dust L_s = 270° seasons [*McCleese et al.*, 2010].

4. Implications for Thermospheric Winter Polar Warming

[11] A closer inspection of Figure 1 shows that the reversal of the meridional temperature gradient in the high-latitude Northern thermosphere was reproduced in all 3 simulations. Although the strong GW-induced cooling lowers down the MLT temperature, it impacts very little the magnitude of the thermospheric winter polar warming measured as a difference between temperatures over the North Pole and at the midlatitude minimum. This can be clearly seen in Figure 2, which presents the temperature cross-sections at p = 0.0002 Pa (≈120 km). The magnitudes of the simulated warming are ∼40 K in the zonally and daily averaged sense for both runs with GWs, which are smaller than ∼60 K in the run without the GW parameterization. Although the shapes of the latitudinal temperature cross-sections are generally preserved in the runs with and without GW heating/cooling (solid red and green lines, correspondingly), the temperatures are 15–20 K lower everywhere and up to 40 K lower in Northern midlatitudes, when the thermal effects of GWs are included. These values are in a good agreement with SPICAM stellar occultation measurements [*Forget et al.*, 2009; *McDunn et al.*, 2010].

[12] For further comparison, we plotted (with the blue dotted line) the night-time (02:00 to 03:00 hours) temperatures derived from the Mars Odyssey (ODY) accelerometer data during aerobraking near perihelion (L_s = 270°) [*Bougher et al.*, 2006, Figure 1]. The corresponding night-side temperature from the run with both dynamical and thermal GW effects is shown by the red dashed line. An excellent agreement between the simulation and measurements is seen except for a small latitudinal region (60°–75°N), where the ∼20 K difference does still exist. The degree of diurnal temperature variations and their latitudinal dependence can be judged from the distance between the solid and dashed red lines in Figure 2. It was confirmed with the modeling, but is also obvious from the plot, that neither the simulation without GWs, nor the run accounting for only the GW drag (that is, without thermal effects) can produce night-time temperatures cold enough to match the aerobraking data. The latter conclusion corroborates the result of *González-Galindo et al.* [2009], whose GCM simulation without GW drag produced the temperatures

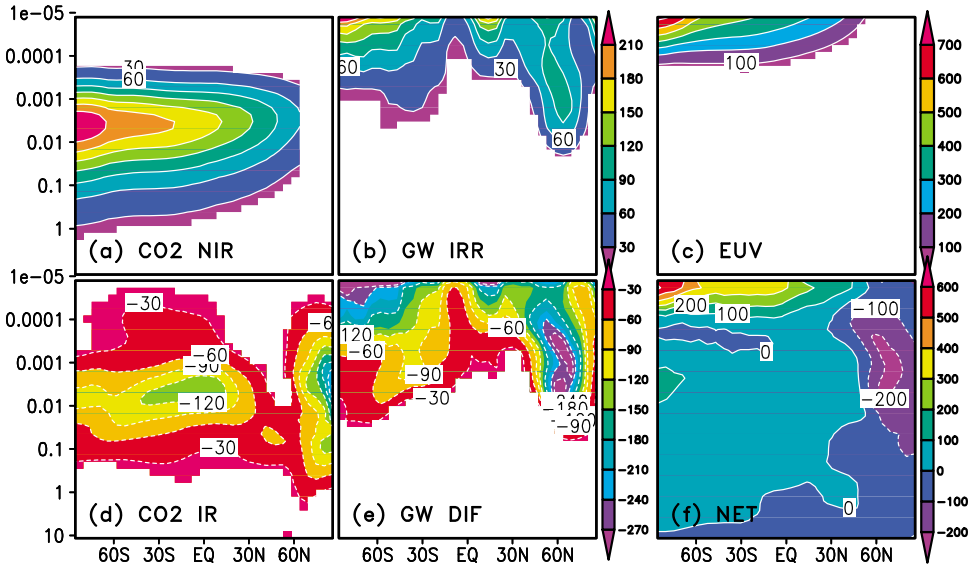

Figure 3. Zonal mean heating and cooling rates (in K sol^{-1}) due to various physical mechanisms: (a) radiative heating by near-IR CO_2 bands; (b) irreversible GW heating; (c) EUV heating by CO_2 molecules; (d) cooling by 15-m bands; (e) differential heating and cooling by GWs; (f) net heating and cooling rates.

30 K higher than the ODY measurements [*González-Galindo et al.*, 2009, Figure 3].

5. Gravity Wave Heating/Cooling Rates

[13] The details of GW-induced thermal forcing, which lead to the significant cooling of the Martian MLT, are illustrated and compared with other diabatic mechanisms in Figure 3. As is expected from equation (1), the GW thermal influence is strong where both wave activity and dissipation are large. The magnitude of irreversible heating due to GW dissipation, Q_{irr}, (Figure 3b) is comparable with the heating due to absorption of solar radiation in near-IR CO_2 bands (both up to 210 K sol^{-1}). However, the two effects are somewhat displaced in height: the former grows with height, while the latter is centered between 0.01 and 0.001 Pa with larger values in the Southern (summer) Hemisphere. (Figure 3a). The differential cooling due to the downward GW-induced heat flux, Q_{diff}, (Figure 3e) is comparable with the CO_2 IR cooling (Figure 3d), and the peak values of Q_{diff} even exceed the latter in the Northern Hemisphere high-latitudes (−270 vs −210 K sol^{-1}). Q_{diff} also increases with height. The regions of enhanced GW heating and cooling generally coincide, and the heating acts to offset the wave cooling. In some sense, this is similar to the behavior of the CO_2 IR cooling that tends to offset the NIR CO_2 heating in the sun-lit atmosphere. The EUV heating (Figure 3c) is the major diabatic factor in the thermosphere, where it is usually offset by molecular heat conduction. However, the latter is still small (less than 30 K sol^{-1}) in the upper portion of our model domain, and, therefore, the differential GW cooling is the main diabatic mechanism that offsets the EUV heating. The dust heating is not shown either since it is located significantly below our region of interest. The distribution of total heating/cooling rates is plotted in Figure 3f. The interhemispheric temperature contrast is compensated by adiabatic cooling associated with rising air in the Southern Hemisphere, and by adiabatic heating induced by downward motions over the North Pole.

6. Summary and Conclusions

[14] We presented a first study of gravity wave (GW)-induced heating and cooling in the Martian atmosphere that employs a GW parameterization fully and interactively incorporated into a 3-D general circulation model (GCM). The spectral nonlinear GW scheme of *Yiğit et al.* [2008] has been implemented into a comprehensive Martian GCM extending from the surface to the lower thermosphere (150–160 km), and simulations for a perpetual Northern winter season (L_s = 270°) have been performed. With respect to our previous study [*Medvedev et al.*, 2011b] that focused only on dynamical effects of GWs, here we additionally implemented a thermospheric UV and EUV heating, and explicitly included heating and cooling rates due to parameterized GWs. Low utilized magnitudes of GWs at the source level corresponding to the background values of observed wave activity [*Creasey et al.*, 2006a] point out to a robustness of the obtained results listed below:

1. Thermal effects of GWs in the mesosphere and lower thermosphere (MLT) are significant, and must be accounted for in the thermal budget. Heating due to an irreversible conversion of gravity wave mechanical energy into heat is comparable to the near-IR CO_2 heating, and the differential cooling due to wave-induced downward heat flux is comparable to the IR CO_2 cooling. These heating and cooling rates are of a similar order with those found by *Parish et al.* [2009] with a 1-D linear wave model for the Martian thermosphere at the same season.

2. Inclusion of GW thermal effects produces a colder MLT in our simulations. This is in agreement with the SPICAM stellar occultation measurements, which revealed temperatures between 100 and 130 km colder than GCMs without GW parameterization could reproduce [*Forget et al.*, 2009; *McDunn et al.*, 2010]. Our experiments predict that

most of the cooling due to GWs takes place in middle- to high-latitudes, especially in the winter hemisphere, where the temperature decreases by up to 45 K. Cooling of the MLT in a similar manner occurs for other seasons as well.

3. The colder simulated MLT is in an excellent agreement with the ODY aerobraking temperature retrievals [*Bougher et al.*, 2006]. On the other hand, our experiments indicate that the magnitude of the thermospheric polar warming is affected by GWs to a smaller extent.

[15] **Acknowledgments.** This work was partially supported by the German Science Foundation (DFG), project HA3261/5, and by AFOSR grant FA9550-07-1-0434.

References

Angelats i Coll, M., F. Forget, M. A. López-Valverde, and F. González-Galindo (2005), The first Mars thermospheric general circulation model: The Martian atmosphere from the ground to 240 km, *Geophys. Res. Lett.*, *32*, L04201, doi:10.1029/2004GL021368.

Becker, E. (2004), Direct heating rates associated with gravity wave saturation, *J. Atmos. Sol. Terr. Phys.*, *66*, 683–696.

Becker, E., and G. Schmitz (2002), Energy deposition and turbulent dissipation owing to gravity waves in the mesosphere, *J. Atmos. Sci.*, *59*, 54–68.

Bougher, S. W., J. M. Bell, J. R. Murphy, M. A. Lopez-Valverde, and P. G. Withers (2006), Polar warming in the Mars thermosphere: Seasonal variations owing to changing insolation and dust distributions, *Geophys. Res. Lett.*, *33*, L02203, doi:10.1029/2005GL024059.

Collins, M., S. R. Lewis, and P. L. Read (1997), Gravity wave drag in a global circulation model of the Martian atmosphere: Parameterization and validation, *Adv. Space Res.*, *19*, 1245–1254.

Creasey, J. E., J. M. Forbes, and D. P. Hinson (2006a), Global and seasonal distribution of gravity wave activity in Mars' lower atmosphere derived from MGS radio occultation data, *Geophys. Res. Lett.*, *33*, L01803, doi:10.1029/2005GL024037.

Creasey, J. E., J. M. Forbes, and G. M. Keating (2006b), Density variability at scales typical of gravity waves observed in Mars' thermosphere by the MGS accelerometer, *Geophys. Res. Lett.*, *33*, L22814, doi:10.1029/2006GL027583.

Forget, F., F. Montmessin, J.-L. Bertaux, F. González-Galindo, S. Lebonnois, E. Quémerais, A. Reberac, E. Dimarellis, and M. A. López-Valverde (2009), Density and temperatures of the upper Martian atmosphere measured by stellar occultations with Mars Express SPICAM, *J. Geophys. Res.*, *114*, E01004, doi:10.1029/2008JE003086.

Fritts, D. C., L. Wang, and R. H. Tolson (2006), Mean and gravity wave structures and variability in the Mars upper atmosphere inferred from Mars Global Surveyor and Mars Odyssey aerobraking densities, *J. Geophys. Res.*, *111*, A12304, doi:10.1029/2006JA011897.

González-Galindo, F., M. A. López-Valverde, M. Angelats i Coll, and F. Forget (2005), Extension of a Martian general circulation model to thermospheric altitudes: UV heating and photochemical models, *J. Geophys. Res.*, *110*, E09008, doi:10.1029/2004JE002312.

González-Galindo, F., F. Forget, M. A. López-Valverde, and M. Angelats i Coll (2009), A ground-to-exosphere Martian general circulation model: 2. Atmosphere during solstice conditions—Thermospheric polar warming, *J. Geophys. Res.*, *114*, E08004, doi:10.1029/2008JE003277.

Hartogh, P., A. S. Medvedev, T. Kuroda, R. Saito, G. Villanueva, A. G. Feofilov, A. A. Kutepov, and U. Berger (2005), Description and climatology of a new general circulation model of the Martian atmosphere, *J. Geophys. Res.*, *110*, E11008, doi:10.1029/2005JE002498.

Heavens, N. G., M. I. Richardson, W. G. Lawson, C. Lee, D. J. McCleese, D. M. Kass, A. Kleinboehl, J. T. Schofild, W. A. Abdou, and J. H. Shirley (2010), Convective instability in the Martian middle atmosphere, *Icarus*, *208*, 574–589,doi:10.1016/j.icarus.2010.03.023.

Joshi, M. M., B. N. Lawrence, and S. R. Lewis (1995), Gravity wave drag in three-dimensional atmospheric models of Mars, *J. Geophys. Res.*, *100*, 21,235–21,245.

Magalhães, J. A., J. T. Schofield, and A. Seiff (1999), Results of the Mars Pathfinder atmospheric structure investigation, *J. Geophys. Res.*, *104*, 8943–8955, doi:10.1029/1998JE900041.

McCleese, D. J., et al. (2010), Structure and dynamics of the Martian lower and middle atmosphere as observed by the Mars Climate Sounder: Seasonal variations in zonal mean temperature, dust, and water ice aerosols, *J. Geophys. Res.*, *115*, E12016, doi:10.1029/2010JE003677.

McDunn, T. L., S. W. Bougher, J. Murphy, M. D. Smith, F. Forget, J.-L. Bertaux, and F. Montmessin (2010), Simulating the density and thermal structure of the middle atmosphere (<80–130 km) of Mars using the MGCM-MTGCM: A comparison with MEX/SPICAM observations, *Icarus*, *206*, 5–17.

Medvedev, A. S., and P. Hartogh (2007), Winter polar warmings and the meridional transport on Mars simulated with a general circulation model, *Icarus*, *186*, 97–110.

Medvedev, A. S., and G. P. Klaassen (2003), Thermal effects of saturating gravity waves in the atmosphere, *J. Geophys. Res.*, *108*(D2), 4040, doi:10.1029/2002JD002504.

Medvedev, A. S., E. Yiğit, and P. Hartogh (2011a), Estimates of gravity wave drag on Mars: Indication of a possible lower thermospheric wind reversal, *Icarus*, *211*, 909–912, doi:10.1016/j.icarus2010.10.013.

Medvedev, A. S., E. Yiğit, P. Hartogh, and E. Becker (2011b), Influence of gravity waves on the Martian atmosphere: General circulation modeling, *J. Geophys. Res.*, *116*, E10004, doi:10.1029/2011JE003848.

Parish, H. F., G. Schubert, M. P. Hickey, and R. L. Walterscheid (2009), Propagation of tropospheric gravity waves into the upper atmosphere of Mars, *Icarus*, *203*, 28–37, doi:10.1016/j.icarus.2009.04.031.

Richards, P. G., J. A. Fennely, and D. G. Torr (1994), EUVAC: A solar EUV flux model for aeronomic calculations, *J. Geophys. Res.*, *99*, 8981–8992.

Torr, M. R., D. G. Torr, R. A. Ong, and H. E. Hinteregger (1979), Ionization frequencies for major thermospheric constituents as a function of solar cycle 21, *Geophys. Res. Lett.*, *6*, 771–774.

Walterscheid, R. L. (1981), Dynamical cooling induced by dissipating internal gravity waves, *Geophys. Res. Lett.*, *8*, 1235–1238.

Yiğit, E., and A. S. Medvedev (2009), Heating and cooling of the thermosphere by internal gravity waves, *Geophys. Res. Lett.*, *36*, L14807, doi:10.1029/2009GL038507.

Yiğit, E., and A. S. Medvedev (2010), Internal gravity waves in the thermosphere during low and high solar activity: Simulation study, *J. Geophys. Res.*, *115*, A00G02, doi:10.1029/2009JA015106.

Yiğit, E., A. D. Aylward, and A. S. Medvedev (2008), Parameterization of the effects of vertically propagating gravity waves for thermosphere general circulation models: Sensitivity study, *J. Geophys. Res.*, *113*, D19106, doi:10.1029/2008JD010135.

Yiğit, E., A. S. Medvedev, A. D. Aylward, P. Hartogh, and M. J. Harris (2009), Modeling the effects of gravity wave momentum deposition on the general circulation above the turbopause, *J. Geophys. Res.*, *114*, D07101, doi:10.1029/2008JD011132.

Yiğit, E., A. S. Medvedev, A. D. Aylward, A. J. Ridley, M. J. Harris, M. B. Moldwin, and P. Hartogh (2012), Dynamical effects of internal gravity waves in the equinoctial thermosphere, *J. Atmos. Sol. Terr. Phys.*, doi:10.1016/j.jastp.2011.11.014, in press.

A. S. Medvedev, Max Planck Institute for Solar System Research, Max-Planck-Str. 2, D-37191 Katlenburg-Lindau, Germany. (medvedev@mps.mpg.de)

E. Yiğit, Department of Atmospheric, Oceanic and Space Sciences, University of Michigan, 1429 Space Research Bldg., Ann Arbor, MI 48109-2143, USA. (erdal@umich.edu)